Published in final edited form as:

Cell Rep. 2018 April 10; 23(2): 485–498. doi:10.1016/j.celrep.2018.03.034.

ADAMTS9-Regulated Pericellular Matrix Dynamics Governs Focal Adhesion-Dependent Smooth Muscle Differentiation

Timothy J. Mead[1], **Yaoyao Du**[1], **Courtney M. Nelson**[1], **Ndeye-Aicha Gueye**[1,2], **Judith Drazba**[3], **Carolyn M. Dancevic**[4], **Mireille Vankemmelbeke**[5], **David J. Buttle**[6], and **Suneel S. Apte**[1,7,*]

[1]Department of Biomedical Engineering, Cleveland Clinic Lerner Research Institute, Cleveland, OH 44195, USA

[2]Department of Obstetrics, Gynecology and Reproductive Sciences, and Women's Health Institute, Cleveland Clinic, Cleveland, OH 44195, USA

[3]Imaging Core, Cleveland Clinic Lerner Research Institute, Cleveland, OH 44195, USA

[4]School of Medicine and Molecular and Medical Research SRC, Faculty of Health, Deakin University, 75 Pigdons Road, Waurn Ponds 3216, VIC, Australia

[5]University of Nottingham, Division of Cancer and Stem Cells, Nottingham City Hospital, Hucknall Road, Nottingham NG5 1PB, United Kingdom

[6]Department of Infection, Immunity & Cardiovascular Disease, University of Sheffield, Beech Hill Road, Sheffield S10 2RX, United Kingdom

SUMMARY

Focal adhesions anchor cells to extracellular matrix (ECM) and direct assembly of a pre-stressed actin cytoskeleton. They act as a cellular sensor and regulator, linking ECM to the nucleus. Here, we identify proteolytic turnover of the anti-adhesive proteoglycan versican as a requirement for maintenance of smooth muscle cell (SMC) focal adhesions. Using conditional deletion in mice, we show that ADAMTS9, a secreted metalloprotease, is required for myometrial activation during late gestation and for parturition. Through knockdown of *ADAMTS9* in uterine SMC, and manipulation of pericellular versican via knockdown or proteolysis, we demonstrate that regulated pericellular matrix dynamics is essential for focal adhesion maintenance. By influencing focal adhesion formation, pericellular versican acts upstream of cytoskeletal assembly and SMC

*Correspondence: aptes@ccf.org.
[7]Lead Contact

SUPPLEMENTAL INFORMATION

Supplemental Information includes Supplemental Experimental Procedures, six figures, three tables, and four videos and can be found with this article online at https://doi.org/10.1016/j.celrep.2018.03.034.

AUTHOR CONTRIBUTIONS

S.S.A. and T.J.M. conceived and designed the experiments and wrote the manuscript. T.J.M., Y.D., C.M.D., and C.M.N. performed the experiments. D.J.B. and M.V. provided recombinant ADAMTS4 and ADAMTS5. N.-A.G. provided human uterine samples. J.D. designed and performed microscopy.

DECLARATION OF INTERESTS

The authors declare no competing interests.

differentiation. Thus, pericellular versican proteolysis by ADAMTS9 balances pro- and anti-adhesive forces to maintain an SMC phenotype, providing a concrete example of the dynamic reciprocity of cells and their ECM.

Graphical abstract

In Brief Mead et al. identify a proteolytic mechanism that actively maintains a pericellular microenvironment conducive to uterine smooth muscle activation prior to parturition. They show that pericellular matrix proteolysis by the secreted metalloprotease ADAMTS9 is crucial for maintenance of focal adhesions in uterine smooth muscle cells, and its absence impairs parturition.

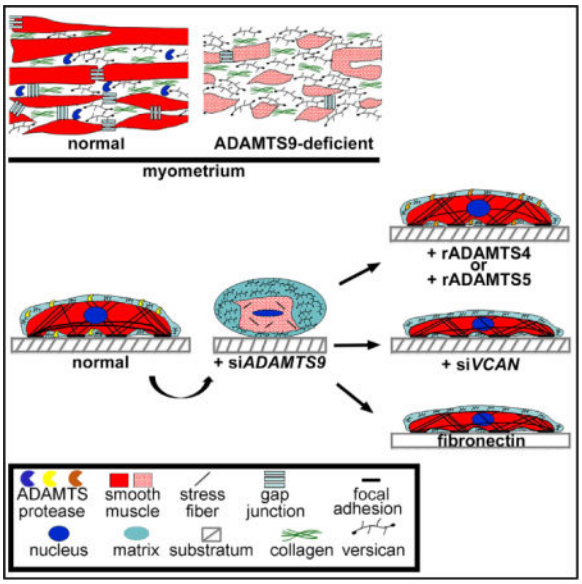

INTRODUCTION

The extracellular matrix (ECM) (Mouw et al., 2014) is a key component of the microenvironment of non-circulating cells, providing diverse inputs to maintain appropriate cellular phenotypes, such as by creating morphogen gradients, moderating cell-cell contacts, and transmitting and modifying mechanical forces (Cho et al., 2017; Mui et al., 2016; Ramirez and Rifkin, 2009). Indeed, cells and their ECM constitute a functional unit whose crosstalk is encapsulated in the concept of ‘‘dynamic reciprocity’’ (Bissell and Aggeler, 1987). Recent work supports a structural and mechanical continuum from the ECM to chromatin via focal adhesions, the actin cytoskeleton, and the nuclear matrix that places cellular tensegrity between the ECM and transcriptional responses to extracellular forces (Cho et al., 2017; Ingber, 2006; Irianto et al., 2016). Secreted and/or cell-surface ECM-degrading proteases are active in numerous contexts (Bonnans et al., 2014) and provide a logical mechanism for mediating cell-matrix adhesion and thus dynamic reciprocity. However, their contribution is not readily evident in steady-state situations. The concept that matrix-degrading proteases could provide a regulatory mechanism for maintenance of cellular phenotypes is emerging, primarily in the context of collagenolysis (Gutiérrez-Fernández et al., 2015; Tang et al., 2013), but is largely unexplored.

Smooth muscle cells (SMCs) ensure contractility of blood vessels, the gut, and, in mammals, the uterus. They provide a classic model for investigating cell phenotype plasticity, expressing specific contractile proteins and having a characteristic spindle shape when fully differentiated; in contrast, dedifferentiated SMCs have reduced contractile proteins and altered morphology (Owens, 2007). The myometrium of the uterine wall comprises SMCs that are electrically coupled by gap junctions for coordinated contraction during parturition (Döring et al., 2006). Enhanced myometrial contractility, connectivity, and heightened responsiveness to parturition hormones (e.g., oxytocin) collectively constitute myometrial ‘‘activation,’’ a hyperdifferentiated state unique to myometrial SMC that occurs prior to parturition (Taggart and Morgan, 2007). SMCs adhere to their ECM via integrin-based focal adhesions (Sun et al., 2016).

A disintegrin-like and metalloproteinase domain with thrombospondin type 1 motifs (ADAMTS) 9 is a highly conserved secreted protease active in cell surface/pericellular matrix proteolysis in diverse contexts revealed using mice with *Adamts9* haploinsufficiency, conditional deletion, or gene trapping (Dubail et al., 2014; Enomoto et al., 2010; McCulloch et al., 2009b). *Adamts9*-null embryos die prior to gastrulation (Benz et al., 2016). ADAMTS9 is one of several ADAMTS proteases that cleave versican, a large, anti-adhesive (Dutt et al., 2006; Sakko et al., 2003; Yamagata and Kimata, 1994; Yamagata et al., 1993), hyaluronan-binding, chondroitin sulfate proteoglycan abundant in pericellular matrix of diverse cells, including SMCs (Evanko et al., 1999). On observing *ADAMTS9* expression in SMCs of several organs, we investigated its function by conditional ablation in mice and knockdown in cultured human uterine SMCs (HUSMCs). The findings suggest that pericellular matrix dynamics can act upstream of focal adhesion assembly and cytoskeletal remodeling to modulate SMC differentiation.

RESULTS

Adamts9 Conditional Deletion in SMCs Leads to Myometrial Anomalies in Late Pregnancy and Impaired Parturition in Mice

β-galactosidase staining of $Adamts9^{LacZ/+}$ tissues and RT-PCR identified *Adamts9* expression in myometrium of the non-gravid and gravid uterus, arterial and intestinal tunica media, human myometrium, and HUSMCs (Figures S1A–S1E), extending previous *in situ* hybridization findings (Jungers et al., 2005). *Adamts9* floxed mice (Dubail et al., 2014) were crossed with *Tagln*-Cre transgenic mice for conditional deletion of *Adamts9* exons 5–8, encoding the catalytic domain (Figures S2A–S2C). Deletion in a subset of SMCs (i.e., uterus, aorta, and intestine) (Holtwick et al., 2002) was confirmed by the *Cre* reporter strain *ROSA-mT/mG* (Muzumdar et al., 2007) (Figures S3B–S3D). Residual uterine *Adamts9* mRNA detectable by RT-PCR of uterus mRNA after conditional deletion (Figures S3B and S3C) may reflect expression by cells other than SMCs (e.g., by microvascular endothelial cells) (Koo and Apte, 2010) or incompletely deleted SMC *Adamts9*.

$Adamts9^{fl/fl}$;*Tagln*-Cre mice of both sexes were externally comparable with $Adamts9^{fl/fl}$ or *Tagln*-Cre littermates and fertile, with unimpaired survival. Although parturition was invariably initiated at term (~19.5 days), 78% of pregnant $Adamts9^{fl/fl}$; *Tagln*-Cre females had arrested or prolonged parturition with embryo retention in the uterus or birth canal or

delivery of dead pups (Table 1). Moreover, 11% of pregnant *Adamts9*$^{fl/+}$*; Tagln*-Cre females had arrested or prolonged parturition, which was not seen in either *Adamts9*$^{fl/fl}$ or *Tagln*-Cre females. Impaired parturition in *Adamts9*$^{fl/fl}$*;Tagln*-Cre females occurred irrespective of the sire or genotypes of the embryos carried, implying a maternal defect.

Mouse myometrium comprises an inner circular layer and outer longitudinal layer soon after birth. By 3 weeks of age, the *Adamts9*$^{fl/fl}$*;Tagln*-Cre uterus was morphologically and histologically similar to *Adamts9*$^{fl/fl}$ and *Tagln*-Cre uterus, implying normal morphogenesis (Figure 1A). In contrast, at the pre-parturition gestational age (G) of 18.5 days (G18.5), thin, non-uniform, and discontinuous myometrial layers of *Adamts9*$^{fl/fl}$*;Tagln*-Cre female mice with reduced collagen contrasted with uniformly stained, densely packed, and organized myometrium of *Adamts9*$^{fl/fl}$ mice (Figures 1A and 1B). No histological differences were seen at G9.5, but by G14.5, increased intercellular space and disruptions in myometrial continuity were evident (Figures 1A and 1B). Transmission electron microscopy (TEM) of G18.5 *Adamts9*$^{fl/fl}$*;Tagln*-Cre myometrium showed widely dispersed collagen fiber bundles with normal collagen fibril morphology and packing density as well as SMC ultrastructure (Figure 1C). A striking increase in amorphous ECM was seen, suggestive of accumulation of non-collagenous components (Figure 1C).

Adamts9-Deficient Myometrium Has Reduced Versican Proteolysis

ADAMTS9, like related family members, cleaves versican at the Glu^{441}-Ala^{442} site within the GAGβ domain and likely elsewhere (Nandadasa et al., 2014; Sandy et al., 2001). Immunofluorescence with a GAGβ domain-specific antibody recognizing the major myometrial splice isoforms V0 and V1 demonstrated enhanced versican staining in G9.5–G18.5 *Adamts9*$^{fl/fl}$*; Tagln*-Cre myometrium but not in 3-week-old non-gravid *Adamts9*$^{fl/fl}$*;Tagln*-Cre uterus (Figure 1D). Conversely, versican cleavage at Glu^{441}-Ala^{442} detected by a neo-epitope antibody anti-DPEAAE^{441} was reduced in gravid *Adamts9*$^{fl/fl}$*;Tagln*-Cre myometrium (Figure 1E). Increased staining of the versican ligand fibronectin was observed in gravid myometrium from *Adamts9*$^{fl/fl}$*;Tagln*-Cre mice (Figure 1F). Western blot demonstrated increased versican V1 in *Adamts9*-deleted uterus and reduced versican processing, identified by a 70 kDa anti-DPEAAE reactive fragment in control uterus (Figure 1G). qRT-PCR showed upregulation of *Vcan* V0 and V1 mRNAs as well as *Fn1* mRNA in *Adamts9*-deleted uterus at G14.5 and G18.5 (Figures 1H and 1I), indicating that their accumulation could result from both reduced proteolysis and increased transcription.

Adamts9 Deletion Impairs Pre-parturition Myometrial SMC Differentiation and Cell-Cell and Cell-ECM Connectivity

SMC contractile proteins ensure myometrial contraction during labor. Smooth muscle a-actin (SMA) and smooth muscle myosin heavy chain (SMMHC) immunostaining showed consistently reduced signal in 3-week-old (non-gravid), G9.5, G14.5, and G18.5 *Adamts9*-deleted myometrium (Figures 2A and 2B). RNAs encoding SMA (*Acta2*), SM22α (*Tagln*), calponin 1 (*Cnn1*), and SMMHC (*Myh11*), which mark the contractile, differentiated SMC phenotype, and a critical regulator of SMC gene expression, myocardin (*Myocd*), were also

reduced (Figure 2C). Western blotting for SMA, SM22α, and SMMHC showed a reduction at G18.5 in *Adamts9*$^{fl/fl}$*;Tagln*-Cre uterus (Figure 2D).

SMC adhesion to ECM, necessary in late pregnancy to support stretch-induced myometrial hypertrophy, is mediated in part by integrin α5 (Williams et al., 2005), which was reduced in *Adamts9*-deficient myometrium (Figure S2E). Collagen VI bridges SMC basement membrane and surrounding ECM, enabling force transmission (Dingemans et al., 2000). As early as G14.5, collagen VI was reduced in the *Adamts9*-deficient myometrium (Figure S2E). Extracellular signal-regulated kinase 1/2 (Erk1/2) is phosphorylated in myometrium during late pregnancy and associated with induction of contractions (Li et al., 2003). *Adamts9*-deficient G18.5 myometrium had reduced pERK1/2 compared with control (Figure S2F). Furthermore, platelet-derived growth factor receptor β (PDGFRβ), which increases during late pregnancy (Bidwell et al., 1995), was reduced in *Adamts9*-deficient myometrium (Figure S2F).

During uterine activation, myometrial SMC achieve heightened connectivity by connexin (Cx) 43 upregulation. Fewer Cx43 gap junctions were seen in G18.5 *Adamts9*$^{fl/fl}$*;Tagln*-Cre myometrium (Figure 2E), western blot showed reduced uterine Cx43 protein (Figure 2F), and qRT-PCR revealed a ~30% reduction of *Gja1* mRNA (encoding Cx43 protein) at G14.5 and G18.5 (Figure 2G). Oxytocin receptor (*Oxtr*) and prostaglandin F2α receptor (*Ptgfr*) are both necessary for hormonal stimulation of uterine contraction (Imamura et al., 2000; Sugimoto et al., 1997). Although unchanged at G14.5, *Oxtr* and *Ptgfr* mRNA were significantly lower in *Adamts9*-deficient G18.5 gravid uterus (Figure 2H). Because G18.5 *Adamts9*$^{fl/fl}$*;Tagln*-Cre myometrial histology appeared to show fewer SMCs compared with *Adamts9*$^{fl/fl}$ myometrium (Figure 1A), proliferation and apoptosis were quantified at G14.5 and G18.5. *Adamts9* deletion did not affect cell proliferation (data not shown), but there were more cleaved caspase-3-positive cells in G18.5 *Adamts9*$^{fl/fl}$*; Tagln*-Cre myometrium (Figures S2G and S2H).

In contrast, aortic histology and ultrastructure were unimpaired in *Adamts9*$^{fl/fl}$*;Tagln*-Cre mice (Figures S3A and S3B), and intestinal structure was normal (Figure S3C). The aorta and intestine did not show altered versican staining or processing, SMC differentiation, or changes in major ECM components (Figures S3A–S3C). Potentially compensating proteases *Adamts1* and *Adamts5* are expressed in aortic SMCs (McCulloch et al., 2009a; Oller et al., 2017) and *Adamts1* in intestinal SMC (Figure S4A). In contrast, *Adamts1* and *Adamts5* were not expressed in non-gravid myometrium and *Adamts1*, but not *Adamts5*, mRNA was detected in gravid myometrium using intragenic *lacZ* (Figure S4A). qRT-PCR revealed unchanged *Adamts1*, *Adamts4*, and *Adamts5* mRNA levels in *Adamts9*$^{fl/fl}$*;Tagln*-Cre aorta (Figure S4B) and increased *Adamts1* mRNA but not *Adamts4*, *Adamts5*, and *Adamts15* mRNA levels in *Adamts9*-deficient gravid uterus (Figure S4C). *Adamts20*, the closest *Adamts9* homolog, was undetectable in mouse aorta or human and mouse uterus (Figure S4D).

ADAMTS9 Is Essential for Phenotype Stability of Cultured HUSMCs

Because myometrial SMCs consistently showed anomalies upon *Adamts9* deletion, we sought the underlying mechanisms in primary HUSMC monolayer cultures, which express

ADAMTS9 (Figure 3A) using short inhibitory RNA oligonucleotides (si*ADAMTS9*) (Figure 3A). Western blotting with anti-DPEAAE detected reduced versican proteolysis in HUSMC cultures after *ADAMTS9* knockdown (Figure 3B). si*ADAMTS9*-transfected HUSMC lost their characteristic spindle shape, with reduction of their surface area, acquisition of a rounded shape, reduced cortical actin, and dramatically fewer stress fibers (Figures 3C and 3D). Extensive spreading and stable adhesion of control siRNA-treated cells was evident in time-lapse microscopy, but si*ADAMTS*9-transfected cells had excessive membrane blebbing and ruffling; with time, these cells rounded, detached from the substratum, and clumped with adjacent cells (Figure 3E; Videos S1 and S2). *ADAMTS9* knockdown led to reduced SMA, SMMHC, and SM22α mRNA and protein (Figures 3F and 3G). Whereas control cells demonstrated well-defined, stress fiber-associated SMA and phospho-myosin light chain staining, both were lost after *ADAMTS*9 knockdown, implying impaired contractility. si*ADAMTS9* inhibited HUSMC adhesion, proliferation, and migration and sensitized HUSMCs to a pro-apoptotic stimulus (Figure S5). Thus, the changes observed in myometrium upon *Adamts9* deletion were replicated in HUSMC by *ADAMTS9* knockdown.

ADAMTS9 Suppression In Vitro Leads to Pericellular ECM Accumulation, Eliminates Focal Adhesions, and Reduces SMC Contractility in Three-Dimensional Cultures

ADAMTS9 is a secreted protease known to bind pericellularly and to target the ECM (Somerville et al., 2003). Because of the dramatic ECM changes in *Adamts9*-deleted myometrium, we investigated the impact of *ADAMTS9* knockdown on the interface between the ventral aspect of adherent HUSMCs (more precisely, their pericellular matrix/glycocalyx) and the substratum using interference reflection microscopy (IRM), an antibody-independent imaging technique (Abercrombie and Dunn, 1975; Curtis, 1964). IRM showed a profound contrast between the substratum contacts made by *ADAMTS9* siRNA-transfected HUSMC and control RNAi-transfected cells (Figure 4A). Dark linear areas indicating focal adhesions (Verschueren, 1985) were numerous in control cells and contrasted with bright areas corresponding to regions where the cell was further removed from the substratum. This contrast was lacking in si*ADAMTS9*-transfected cells, which had a preponderance of gray signal, indicating an intermediate adhesion state described as close contacts (Verschueren, 1985) with the substratum (Figures 4A and 4B; Videos S3 and S4). Consistent with this, staining of focal adhesion components vinculin, talin, phospho (p)-paxillin, and p-FAK was no longer clustered in focal adhesions in the si*ADAMTS9*-transfected SMCs (Figure 4C). Furthermore, vinculin and talin, as well as β1 integrin and filamin, which are components of the SMC ECM-signal transduction machinery (Taggart and Morgan, 2007), were all reduced in western blot analysis of si*ADAMTS*9-transfected HUSMCs (Figure 4D). Because emerging evidence suggests a linkage of nuclear matrix and shape with cellular tensegrity, we examined nuclear area and nuclear aspect ratio in si*ADAMTS*9-transfected HUSMCs and found both to be significantly altered (Figures 4E and 4F).

An *in vitro* three-dimensional model for cell contractility showed that si*ADAMTS9*-transfected HUSMC-containing collagen gels contracted 2-fold less than control siRNA-treated HUSMC-containing gels (Figures 5A and 5B), consistent with their observed

reduction of focal adhesions and contractile proteins. Treatment of si*ADAMTS9*-transfected HUSMCs with exogenous ADAMTS4 and ADAMTS5, which cleave versican (Longpré et al., 2009; Sandy et al., 2001) restored collagen gel contractility (Figures 5A and 5B). Furthermore, exogenous ADAMTS4 and ADAMTS5 largely prevented rounding and clumping of si*ADAMTS9*-transfected HUSMCs, led to reappearance of focal adhesions (Figures 5C and 5D), and restored the characteristic SMC spindle shape (Figure S6A).

Versican-degrading proteases, including ADAMTS9, which binds to the cell surface/pericellular matrix (Somerville et al., 2003), could potentially affect turnover of the versican-rich SMC pericellular matrix to influence formation of focal adhesions. Therefore, we asked if the focal adhesion anomalies observed after *ADAMTS9* knockdown were modified by concurrent *VCAN* knockdown. In contrast to *ADAMTS9* knockdown, which in co-transfected cells was typically about 50% (Figure 6A), near-complete *VCAN* knockdown was achieved (Figure 6B) and thus likely affected all cells with *ADAMTS9* knockdown. Interestingly, and presently unexplained, *VCAN* mRNA was increased in si*ADAMTS9*-treated cells (Figure 6B). A red blood cell exclusion assay, which outlines the pericellular matrix, showed an increase in HUSMC pericellular matrix after *ADAMTS9* knockdown (Figures 6C and 6D). In contrast, minimal pericellular matrix was observed in HUSMCs after control siRNA or si*VCAN* transfection (Figures 6C and 6D), indicating low levels of steady-state versican at the cell surface and implying rapid turnover by ADAMTS9. The accumulated pericellular matrix observed after si*ADAMTS9* transfection was restored to baseline by simultaneous *VCAN* knockdown, also implying that versican was a major constituent of the accumulated pericellular ECM (Figures 6C and 6D).

To ask whether versican accumulation in HUSMC pericellular matrix after *ADAMTS9* knockdown adversely affected focal adhesions, these co-transfections were followed by IRM to visualize cell-matrix interactions. si*VCAN* alone had no effect on cell morphology or focal adhesions compared with control siRNA (Figure 6E). Thus, whereas excess versican-rich pericellular matrix after *ADAMTS9* knockdown may interfere with focal adhesions, *VCAN* knockdown alone did not, suggesting low steady-state versican levels in pericellular matrix (Figures 6C and 6D). Importantly, concomitant knockdown of *VCAN* in si*ADAMTS9*-transfected cells led to reappearance of focal adhesions (Figures 6E and 6F). Thus, reduced versican turnover at the cell surface upon *ADAMTS9* knockdown, resulting in versican accumulation and increased pericellular matrix, could explain impairment of focal adhesions. To ask whether a high density of adhesive sites mitigated against the effect of versican accumulation, we knocked down *ADAMTS9* in HUSMCs plated on fibronectin and observed improved morphology and adhesion than on tissue culture plastic (Figures S6B and S6C).

DISCUSSION

Conditional *Adamts9* deletion in SMCs unexpectedly perturbed myometrial ECM remodeling and led to SMC dedifferentiation. The combination of reduced expression of contractile proteins, impeded SMC coupling by gap junctions necessary for synchronous uterine contraction, and reduced expression of parturition hormone receptors impeded the process of myometrial activation and impaired parturition. Indeed, it was previously shown

that genetic disruption of Cx43, which forms gap junctions in uterine SMCs, or of oxytocin and prostaglandin F2 receptors impaired parturition in mice (Döring et al., 2006; Sugimoto et al., 1997). The myometrial versican-rich ECM resulting from *Adamts9* deletion may have also contributed to a relative reduction of collagen, which is required both for stretch-mediated SMC differentiation and for mechanical transmission of uterine contractions (Williams et al., 2005). ADAMTS9 thus represents an evolutionarily crucial molecule, as it is required for both mammalian morphogenesis (Benz et al., 2016; Dubail et al., 2014; Enomoto et al., 2010; Nandadasa et al., 2015) and, as shown here, reproduction. A recent comparison of the myometrial transcriptome in women with spontaneous term labor versus those with arrested dilatation during labor identified *ADAMTS9* mRNA overexpression as an anomaly in the latter (Chaemsaithong et al., 2013). Taken together with the present findings, we conclude that an optimal level of ADAMTS9 activity is required in myometrium to ensure proper parturition. The contrasting lack of impact of *Adamts9* deletion on aorta and intestine SMCs can be explained in part by ADAMTS redundancy (McCulloch et al., 2009a; Oller et al., 2017; Sandy et al., 2001), which compensates for the absence of ADAMTS9. Furthermore, pregnancy presents a dramatic challenge to the myometrium that elicited the observed uterine phenotype, whereas the aorta, for example, was not challenged, such as by inducing high arterial pressure. It will be of interest to determine whether pericellular matrix turnover by ADAMTS proteases is a general requirement for maintenance of the SMC phenotype.

ADAMTS9 knockdown in cultured HUSMCs identified several cellular correlates of impaired myometrial activation and suggests that myometrial activation and differentiation depend on an appropriate cell-matrix interface. Altered cell and nuclear shape and reduced contractility of uterine SMCs reflected lack of cytoskeletal organization and downregulation of the HUSMC contractile machinery, respectively. Because ADAMTS9 is a secreted metalloprotease known to localize to the cell surface, we investigated the impact on pericellular matrix and focal adhesions. Our studies strongly support accumulation of versican, an anti-adhesive molecule (Sakko et al., 2001; Yamagata and Kimata, 1994; Yamagata et al., 1989), at the cell surface as a mechanism of focal adhesion loss in *ADAMTS9*-transfected cells. Versican accumulation appears to alter the balance of pro- and anti-adhesive molecules at the cell-matrix interface. This conclusion is supported by restoration of focal adhesions after *VCAN* knockdown in si*ADAMTS9*-transfected cells and their improved morphology on a fibronectin substratum, which provides a higher density of integrin ligand.

Consistent with an anti-adhesive role, versican is typically excluded from focal contacts (Yamagata et al., 1993). Its anti-adhesive effect was implicated in formation of podosomes rather than focal adhesions in transformed MG63 cells, in which focal adhesions and stress fibers were restored by versican knockdown (Yamagata and Kimata, 1994). Furthermore, induced overexpression of the *VCAN* isoform V3, which lacks the glycosylated domains that endow versican with its anti-adhesive effect, enhanced focal adhesion formation (Lemire et al., 2002). Previously, it was shown that pericellular versican-rich matrix was rapidly turned over in arterial SMC, although the mechanisms were unknown, and it was implicated in SMC rounding (Evanko et al., 1999). Our data thus support a model in which versican produced by uterine SMCs undergoes proteolysis by ADAMTS9 (or other versican-

degrading proteases) in order to maintain an optimal pericellular matrix volume and/or composition for formation of focal adhesions; in the absence of ADAMTS9, versican accumulates in HUSMCs and myometrium, and a de-adhesive state results. Although our studies do not formally consider or exclude other possible ADAMTS9 substrates in the observed effects, the reversal of the *ADAMTS9* siRNA effect in HUSMCs by concurrent *VCAN* knockdown strongly suggests that versican is a major component of the accumulated pericellular matrix in these cells that underlies impaired focal adhesions.

Focal adhesions and cytoskeleton are interdependent (Livne and Geiger, 2016). Indeed, restoration of focal adhesions by exogenous proteases or concurrent *VCAN* knockdown (i.e., acting external to the cell) ameliorated the impact of *ADAMTS9* siRNA on HUSMC contractility. Emerging evidence suggests that ECM is coupled to the nucleus via focal adhesions, actin cytoskeleton, and the LINC complex (linker of nucleoskeleton to the cytoskeleton) and that the resulting cell and nuclear pre-stress is important for transcriptional regulation (Chambliss et al., 2013; Cho et al., 2017; Guilluy et al., 2014; Irianto et al., 2016; Plessner et al., 2015). We suggest that elimination of focal adhesions upon ADAMTS9 depletion and the resulting altered cell pre-stress and nuclear shape are responsible, at least in part, for the altered transcriptional program of ADAMTS9-deficient SMC.

How does accumulated versican impair focal adhesions? Previous work showed that initial interactions of cells with rigid substrates are mediated by a hydrated pericellular coat comprising hyaluronan and aggregating proteoglycans such as versican and are weak. Subsequently, stable adhesions are formed via integrin engagement of ECM (Cohen et al., 2006; Zimmerman et al., 2002). This transition from weak to strong adhesion is likely to be recapitulated serially as cells divide or move in monolayer culture, dismantling existing focal adhesions and forming new ones. Cell adhesion is thus a dynamic, reversible process, with de-adhesion involving transition from a spread state of strong adhesion to weak adherence typified by cell rounding (Murphy-Ullrich, 2001). We propose that progressive accumulation of pericellular ECM in the absence of ADAMTS9 prevents effective formation of new focal adhesions, so that only the weak initial contacts persist, as supported by the IRM imaging and videos. Eventually, the accumulated ‘‘soft’’ hydrated ECM between the cell and adhesive surface promotes cell rounding as observed here upon *ADAMTS9* knockdown.

Regulation of cell adhesion is relevant to physiological processes such as tissue morphogenesis and regeneration and diseases such as inflammation, cancer, and metastasis. Although the main interface between cells and their surroundings is the pericellular matrix, constituting the *de facto* microenvironment, its dynamics are poorly understood, understudied in the regulation of cell adhesion, and the underlying mechanisms are virtually unknown. The HA-versican matrix, similar to that of the provisional ECM of the embryo, comprises the pericellular ECM of most mesenchymal cells (Evanko et al., 1999; Hattori et al., 2011). It is readily accessible to cellular proteolysis and is known to be dynamic (Evanko et al., 1999), but specific proteases involved have not been identified. Previously, in *Adamts9*$^{GT/GT}$ mice, an *Adamts9* hypomorphic mutant arising from gene trapping, impaired vascular SMC differentiation and failure of morphogenetically crucial orthogonal rotation was associated with reduced versican proteolysis in SMC and adjacent Wharton’s jelly

(Nandadasa et al., 2015). As in the myometrium, ADAMTS9 appears to be the major versican-degrading ADAMTS protease in the umbilical cord, and electron microscopy of *Adamts9*$^{GT/GT}$ umbilical cords (Nandadasa et al., 2015) showed a similar excess of amorphous ECM around SMCs, as observed here. Other work had shown that reduced versican proteolysis in *Adamts5*-deficient dermal fibroblasts led to accumulation of pericellular versican and to myofibroblast transition *in vitro*, which was ameliorated genetically by *Vcan* haploinsufficiency (Hattori et al., 2011). Correspondingly, overexpression of versican by transfection in dermal fibroblasts led to myofibroblast characteristics, whereas versican-deficient fibroblasts showed reduced SMA and contractility (Carthy et al., 2015; Hattori et al., 2011). Thus pericellular versican appears to profoundly influence cell behavior, but its effects may be cell type specific.

In conclusion, little attention was previously given to the possibility that focal adhesion formation could be influenced from outside the cell by pericellular matrix dynamics, despite intimate association of nearly all non-epithelial adherent cells with this matrix. This paradigm, in which a secreted protease balances pro- and anti-adhesive forces at the cell surface to influence maintenance of focal adhesions, is a concrete example of the dynamic reciprocity of cells and their matrix.

EXPERIMENTAL PROCEDURES

Conditional Ablation of *Adamts9* in SMCs

Adamts9$^{lacZ/+}$ mice (RRID: MGI:4418867) and the *Adamts9*^{fl} allele (B6[SJL]-*Adamts9*$^{tm1.1Apte}$/J; RRID: MGI:5603200) were previously described (Dubail et al., 2014; Koo et al., 2010). *Adamts9*$^{fl/fl}$*;Tagln*-Cre mice were generated by crossing *Adamts9*$^{fl/fl}$ mice with *Tagln*-Cre transgenic mice (B6.Cg-Tg [*Tagln*-Cre]1Her/J; Jackson Laboratories, Bar Harbor, ME), which express *Cre* recombinase driven by the smooth muscle 22α promoter (Holtwick et al., 2002). Genotyping is described in Supplemental Experimental Procedures. In all experiments, *Tagln*-Cre or *Adamts9*$^{fl/fl}$ littermates of *Adamts9*$^{fl/fl}$*;Tagln*-Cre mice were used as controls. Gt(ROSA)26Sortm4(*ACTB*-tdTomato,-EGFP)Luo/J reporter mice for Cre activity (Muzumdar et al., 2007) (designated here as *ROSA-mT/mG*) were obtained from Jackson Laboratories. All procedures were approved by the Institutional Animal Care and Use Committee of the Cleveland Clinic.

Tissue Analysis

Dissected tissues were fixed in 4% paraformaldehyde in PBS at 4°C overnight, followed by paraffin embedding. Sections 7 μm thick were used for H&E staining, Masson trichrome staining for collagen, and immunofluorescence with primary antibodies (Table S1), followed by secondary goat anti-mouse or goat anti-rabbit antibody as appropriate with citrate retrieval. Immunofluorescence, β-galactosidase staining, TEM, and western blotting are described in Supplemental Experimental Procedures.

Cell Culture and siRNA Treatment

HUSMCs (cc-2562; Lonza, Basel, Switzerland) were maintained on tissue culture plastic in HUSMC complete media (SmGM-2 medium [cc-3181; Lonza] supplemented with 5% fetal

bovine serum, growth factors [cc-4149; Lonza]), 100 U/mL penicillin, and 100 mg/mL streptomycin. Cells in passages 3–8 were used for all experiments. HUSMCs in six-well plates were transfected with *ADAMTS9* siRNA (SASI_Hs02_00371041; Sigma-Aldrich), *VCAN* siRNA (Silencer select s229335; Ambion, Waltham, MA), or control siRNA (SIC001; Sigma-Aldrich) using Lipofectamine RNAiMAX (13778; Invitrogen, Carlsbad, CA) upon achieving 60% confluence and harvested 48 hr after transfection. For rescue experiments, ADAMTS4 or ADAMTS5 at 0.1 U/mL (Vankemmelbeke et al., 2003) was added at the time of transfection and at 24 hr or cells were plated on fibronectin (Supplemental Experimental Procedures).

IRM

Monolayers of HUSMCs were grown and siRNA-transfected. The cells were re-plated on a glass-bottom dish (D-29-10-0-N; Cellvis, Mountain View, CA) and imaged 24 hr later in a heat/CO_2-controlled environmental chamber on an inverted Leica SP8 confocal microscope. Images were collected using an HCX PL APO 40×/1.25 NA oil immersion objective at zoom 1, 488 nm excitation, the PMT window collecting light from 450–530 nm (reflection imaging), and the pinhole wide open (600 μm).

Statistics

All values are expressed as mean ± SEM. Unpaired two-tailed Student's t tests were used to assess statistical significance.

Study Approval

All experimental procedures involving animals in this study were reviewed and approved by the Cleveland Clinic IACUC. Human myometrium and aorta were collected prospectively from discarded tissue with the approval of the Cleveland Clinic Institutional Review Board (study numbers 14-1603 and 14-2378, respectively).

Supplementary Material

Refer to Web version on PubMed Central for supplementary material.

Acknowledgments

Funding was provided by the National Heart, Lung, and Blood Institute (NHLBI) Program of Excellence in Glycosciences (award HL107147 to S.S.A.), the National Institute of Arthritis and Musculoskeletal and Skin Diseases (NIAMS) (award F32AR063548 to T.J.M.), Sabrina's Foundation (to S.S.A.), and the David and Lindsay Morgenthaler Postdoctoral Fellowship (to T.J.M.). S.S.A. is supported in part by the American Heart Association-Paul G. Allen Frontiers Group Distinguished Investigator Award. This work used a Leica SP8 confocal microscope that was purchased with funding from NIH Shared Instrument Grant (SIG) 1S10OD019972-01. We thank the members of the Apte laboratory for valuable comments.

References

Abercrombie M, Dunn GA. Adhesions of fibroblasts to substratum during contact inhibition observed by interference reflection microscopy. Exp Cell Res. 1975; 92:57–62. [PubMed: 1169157]

Benz BA, Nandadasa S, Takeuchi M, Grady RC, Takeuchi H, LoPilato RK, Kakuda S, Somerville RPT, Apte SS, Haltiwanger RS, Holdener BC. Genetic and biochemical evidence that gastrulation

defects in Pofut2 mutants result from defects in ADAMTS9 secretion. Dev Biol. 2016; 416:111–122. [PubMed: 27297885]

Bidwell MC, Eitzman BA, Walmer DK, McLachlan JA, Gray KD. Analysis of messenger ribonucleic acid and protein for the ligands and receptors of the platelet-derived growth factor signaling pathway in the placenta, extraembryonic membranes, and uterus during the latter half of murine gestation. Endocrinology. 1995; 136:5189–5201. [PubMed: 7588258]

Bissell MJ, Aggeler J. Dynamic reciprocity: how do extracellular matrix and hormones direct gene expression? Prog Clin Biol Res. 1987; 249:251–262. [PubMed: 3671428]

Bonnans C, Chou J, Werb Z. Remodelling the extracellular matrix in development and disease. Nat Rev Mol Cell Biol. 2014; 15:786–801. [PubMed: 25415508]

Carthy JM, Meredith AJ, Boroomand S, Abraham T, Luo Z, Knight D, McManus BM. Versican V1 overexpression induces a myofibroblast-like phenotype in cultured fibroblasts. PLoS ONE. 2015; 10:e0133056. [PubMed: 26176948]

Chaemsaithong P, Madan I, Romero R, Than NG, Tarca AL, Draghici S, Bhatti G, Yeo L, Mazor M, Kim CJ, et al. Characterization of the myometrial transcriptome in women with an arrest of dilatation during labor. J Perinat Med. 2013; 41:665–681. [PubMed: 23893668]

Chambliss AB, Khatau SB, Erdenberger N, Robinson DK, Hodzic D, Longmore GD, Wirtz D. The LINC-anchored actin cap connects the extracellular milieu to the nucleus for ultrafast mechanotransduction. Sci Rep. 2013; 3:1087. [PubMed: 23336069]

Cho S, Irianto J, Discher DE. Mechanosensing by the nucleus: from pathways to scaling relationships. J Cell Biol. 2017; 216:305–315. [PubMed: 28043971]

Cohen M, Kam Z, Addadi L, Geiger B. Dynamic study of the transition from hyaluronan- to integrin-mediated adhesion in chondrocytes. EMBO J. 2006; 25:302–311. [PubMed: 16407968]

Curtis AS. The mechanism of adhesion of cells to glass. A study by interference reflection microscopy. J Cell Biol. 1964; 20:199–215. [PubMed: 14126869]

Dingemans KP, Teeling P, Lagendijk JH, Becker AE. Extracellular matrix of the human aortic media: an ultrastructural histochemical and immunohistochemical study of the adult aortic media. Anat Rec. 2000; 258:1–14. [PubMed: 10603443]

Döring B, Shynlova O, Tsui P, Eckardt D, Janssen-Bienhold U, Hofmann F, Feil S, Feil R, Lye SJ, Willecke K. Ablation of connexin43 in uterine smooth muscle cells of the mouse causes delayed parturition. J Cell Sci. 2006; 119:1715–1722. [PubMed: 16595547]

Dubail J, Aramaki-Hattori N, Bader HL, Nelson CM, Katebi N, Matuska B, Olsen BR, Apte SS. A new Adamts9 conditional mouse allele identifies its non-redundant role in interdigital web regression. Genesis. 2014; 52:702–712. [PubMed: 24753090]

Dutt S, Kléber M, Matasci M, Sommer L, Zimmermann DR. Versican V0 and V1 guide migratory neural crest cells. J Biol Chem. 2006; 281:12123–12131. [PubMed: 16510447]

Enomoto H, Nelson CM, Somerville RPT, Mielke K, Dixon LJ, Powell K, Apte SS. Cooperation of two ADAMTS metalloproteases in closure of the mouse palate identifies a requirement for versican proteolysis in regulating palatal mesenchyme proliferation. Development. 2010; 137:4029–4038. [PubMed: 21041365]

Evanko SP, Angello JC, Wight TN. Formation of hyaluronan-and versican-rich pericellular matrix is required for proliferation and migration of vascular smooth muscle cells. Arterioscler Thromb Vasc Biol. 1999; 19:1004–1013. [PubMed: 10195929]

Guilluy C, Osborne LD, Van Landeghem L, Sharek L, Superfine R, Garcia-Mata R, Burridge K. Isolated nuclei adapt to force and reveal a mechanotransduction pathway in the nucleus. Nat Cell Biol. 2014; 16:376–381. [PubMed: 24609268]

Gutiérrez-Fernández A, Soria-Valles C, Osorio FG, Gutiérrez-Abril J, Garabaya C, Aguirre A, Fueyo A, Fernández-García MS, Puente XS, López-Otín C. Loss of MT1-MMP causes cell senescence and nuclear defects which can be reversed by retinoic acid. EMBO J. 2015; 34:1875–1888. [PubMed: 25991604]

Hattori N, Carrino DA, Lauer ME, Vasanji A, Wylie JD, Nelson CM, Apte SS. Pericellular versican regulates the fibroblast-myofibroblast transition: a role for ADAMTS5 protease-mediated proteolysis. J Biol Chem. 2011; 286:34298–34310. [PubMed: 21828051]

Holtwick R, Gotthardt M, Skryabin B, Steinmetz M, Potthast R, Zetsche B, Hammer RE, Herz J, Kuhn M. Smooth muscle-selective deletion of guanylyl cyclase-A prevents the acute but not chronic effects of ANP on blood pressure. Proc Natl Acad Sci U S A. 2002; 99:7142–7147. [PubMed: 11997476]

Imamura T, Luedke CE, Vogt SK, Muglia LJ. Oxytocin modulates the onset of murine parturition by competing ovarian and uterine effects. Am J Physiol Regul Integr Comp Physiol. 2000; 279:R1061–R1067. [PubMed: 10956266]

Ingber DE. Cellular mechanotransduction: putting all the pieces together again. FASEB J. 2006; 20:811–827. [PubMed: 16675838]

Irianto J, Pfeifer CR, Xia Y, Discher DE. SnapShot: mechanosensing matrix. Cell. 2016; 165:1820–1820.e1. [PubMed: 27315485]

Jungers KA, Le Goff C, Somerville RP, Apte SS. Adamts9 is widely expressed during mouse embryo development. Gene Expr Patterns. 2005; 5:609–617. [PubMed: 15939373]

Koo BH, Apte SS. Cell-surface processing of the metalloprotease pro-ADAMTS9 is influenced by the chaperone GRP94/gp96. J Biol Chem. 2010; 285:197–205. [PubMed: 19875450]

Koo BH, Coe DM, Dixon LJ, Somerville RP, Nelson CM, Wang LW, Young ME, Lindner DJ, Apte SS. ADAMTS9 is a cell-autonomously acting, anti-angiogenic metalloprotease expressed by microvascular endothelial cells. Am J Pathol. 2010; 176:1494–1504. [PubMed: 20093484]

Lemire JM, Merrilees MJ, Braun KR, Wight TN. Overexpression of the V3 variant of versican alters arterial smooth muscle cell adhesion, migration, and proliferation in vitro. J Cell Physiol. 2002; 190:38–45. [PubMed: 11807809]

Li Y, Je HD, Malek S, Morgan KG. ERK1/2-mediated phosphorylation of myometrial caldesmon during pregnancy and labor. Am J Physiol Regul Integr Comp Physiol. 2003; 284:R192–R199. [PubMed: 12388473]

Livne A, Geiger B. The inner workings of stress fibers—from contractile machinery to focal adhesions and back. J Cell Sci. 2016; 129:1293–1304. [PubMed: 27037413]

Longpré JM, McCulloch DR, Koo BH, Alexander JP, Apte SS, Leduc R. Characterization of proADAMTS5 processing by proprotein convertases. Int J Biochem Cell Biol. 2009; 41:1116–1126. [PubMed: 18992360]

McCulloch DR, Le Goff C, Bhatt S, Dixon LJ, Sandy JD, Apte SS. Adamts5, the gene encoding a proteoglycan-degrading metalloprotease, is expressed by specific cell lineages during mouse embryonic development and in adult tissues. Gene Expr Patterns. 2009a; 9:314–323. [PubMed: 19250981]

McCulloch DR, Nelson CM, Dixon LJ, Silver DL, Wylie JD, Lindner V, Sasaki T, Cooley MA, Argraves WS, Apte SS. ADAMTS metalloproteases generate active versican fragments that regulate interdigital web regression. Dev Cell. 2009b; 17:687–698. [PubMed: 19922873]

Mouw JK, Ou G, Weaver VM. Extracellular matrix assembly: a multiscale deconstruction. Nat Rev Mol Cell Biol. 2014; 15:771–785. [PubMed: 25370693]

Mui KL, Chen CS, Assoian RK. The mechanical regulation of integrin-cadherin crosstalk organizes cells, signaling and forces. J Cell Sci. 2016; 129:1093–1100. [PubMed: 26919980]

Murphy-Ullrich JE. The de-adhesive activity of matricellular proteins: is intermediate cell adhesion an adaptive state? J Clin Invest. 2001; 107:785–790. [PubMed: 11285293]

Muzumdar MD, Tasic B, Miyamichi K, Li L, Luo L. A global double-fluorescent Cre reporter mouse. Genesis. 2007; 45:593–605. [PubMed: 17868096]

Nandadasa S, Foulcer S, Apte SS. The multiple, complex roles of versican and its proteolytic turnover by ADAMTS proteases during embryogenesis. Matrix Biol. 2014; 35:34–41. [PubMed: 24444773]

Nandadasa S, Nelson CM, Apte SS. ADAMTS9-mediated extracellular matrix dynamics regulates umbilical cord vascular smooth muscle differentiation and rotation. Cell Rep. 2015; 11:1519–1528. [PubMed: 26027930]

Oller J, Méndez-Barbero N, Ruiz EJ, Villahoz S, Renard M, Canelas LI, Briones AM, Alberca R, Lozano-Vidal N, Hurlé MA, et al. Nitric oxide mediates aortic disease in mice deficient in the metalloprotease Adamts1 and in a mouse model of Marfan syndrome. Nat Med. 2017; 23:200–212. [PubMed: 28067899]

Owens GK. Molecular control of vascular smooth muscle cell differentiation and phenotypic plasticity. Novartis Found Symp. 2007; 283:174–191. [PubMed: 18300422]

Plessner M, Melak M, Chinchilla P, Baarlink C, Grosse R. Nuclear F-actin formation and reorganization upon cell spreading. J Biol Chem. 2015; 290:11209–11216. [PubMed: 25759381]

Ramirez F, Rifkin DB. Extracellular microfibrils: contextual platforms for TGFbeta and BMP signaling. Curr Opin Cell Biol. 2009; 21:616–622. [PubMed: 19525102]

Sakko AJ, Ricciardelli C, Mayne K, Tilley WD, Lebaron RG, Horsfall DJ. Versican accumulation in human prostatic fibroblast cultures is enhanced by prostate cancer cell-derived transforming growth factor beta1. Cancer Res. 2001; 61:926–930. [PubMed: 11221884]

Sakko AJ, Ricciardelli C, Mayne K, Suwiwat S, LeBaron RG, Marshall VR, Tilley WD, Horsfall DJ. Modulation of prostate cancer cell attachment to matrix by versican. Cancer Res. 2003; 63:4786–4791. [PubMed: 12941795]

Sandy JD, Westling J, Kenagy RD, Iruela-Arispe ML, Verscharen C, Rodriguez-Mazaneque JC, Zimmermann DR, Lemire JM, Fischer JW, Wight TN, Clowes AW. Versican V1 proteolysis in human aorta in vivo occurs at the Glu441-Ala442 bond, a site that is cleaved by recombinant ADAMTS-1 and ADAMTS-4. J Biol Chem. 2001; 276:13372–13378. [PubMed: 11278559]

Somerville RP, Longpre JM, Jungers KA, Engle JM, Ross M, Evanko S, Wight TN, Leduc R, Apte SS. Characterization of ADAMTS-9 and ADAMTS-20 as a distinct ADAMTS subfamily related to Caenorhabditis elegans GON-1. J Biol Chem. 2003; 278:9503–9513. [PubMed: 12514189]

Sugimoto Y, Yamasaki A, Segi E, Tsuboi K, Aze Y, Nishimura T, Oida H, Yoshida N, Tanaka T, Katsuyama M, et al. Failure of parturition in mice lacking the prostaglandin Freceptor. Science. 1997; 277:681–683. [PubMed: 9235889]

Sun Z, Guo SS, Fässler R. Integrin-mediated mechanotransduction. J Cell Biol. 2016; 215:445–456. [PubMed: 27872252]

Taggart MJ, Morgan KG. Regulation of the uterine contractile apparatus and cytoskeleton. Semin Cell Dev Biol. 2007; 18:296–304. [PubMed: 17582796]

Tang Y, Rowe RG, Botvinick EL, Kurup A, Putnam AJ, Seiki M, Weaver VM, Keller ET, Goldstein S, Dai J, et al. MT1-MMP-dependent control of skeletal stem cell commitment via a β1-integrin/YAP/TAZ signaling axis. Dev Cell. 2013; 25:402–416. [PubMed: 23685250]

Vankemmelbeke MN, Jones GC, Fowles C, Ilic MZ, Handley CJ, Day AJ, Knight CG, Mort JS, Buttle DJ. Selective inhibition of ADAMTS-1, -4 and -5 by catechin gallate esters. Eur J Biochem. 2003; 270:2394–2403. [PubMed: 12755694]

Verschueren H. Interference reflection microscopy in cell biology: methodology and applications. J Cell Sci. 1985; 75:279–301. [PubMed: 3900106]

Williams SJ, White BG, MacPhee DJ. Expression of alpha5 integrin (Itga5) is elevated in the rat myometrium during late pregnancy and labor: implications for development of a mechanical syncytium. Biol Reprod. 2005; 72:1114–1124. [PubMed: 15635129]

Yamagata M, Kimata K. Repression of a malignant cell-substratum adhesion phenotype by inhibiting the production of the anti-adhesive proteoglycan, PG-M/versican. J Cell Sci. 1994; 107:2581–2590. [PubMed: 7531202]

Yamagata M, Suzuki S, Akiyama SK, Yamada KM, Kimata K. Regulation of cell-substrate adhesion by proteoglycans immobilized on extracellular substrates. J Biol Chem. 1989; 264:8012–8018. [PubMed: 2470739]

Yamagata M, Saga S, Kato M, Bernfield M, Kimata K. Selective distributions of proteoglycans and their ligands in pericellular matrix of cultured fibroblasts. Implications for their roles in cell-substratum adhesion. J Cell Sci. 1993; 106:55–65. [PubMed: 8270643]

Zimmerman E, Geiger B, Addadi L. Initial stages of cell-matrix adhesion can be mediated and modulated by cell-surface hyaluronan. Biophys J. 2002; 82:1848–1857. [PubMed: 11916844]

Highlights

- ADAMTS9, a secreted metalloproteinase, is required for parturition in mice
- *ADAMTS9* siRNA impairs focal adhesion formation in uterine smooth muscle cells
- ADAMTS9 ensures focal adhesion formation via pericellular versican turnover
- Pericellular matrix proteolysis is a crucial regulator of focal adhesions

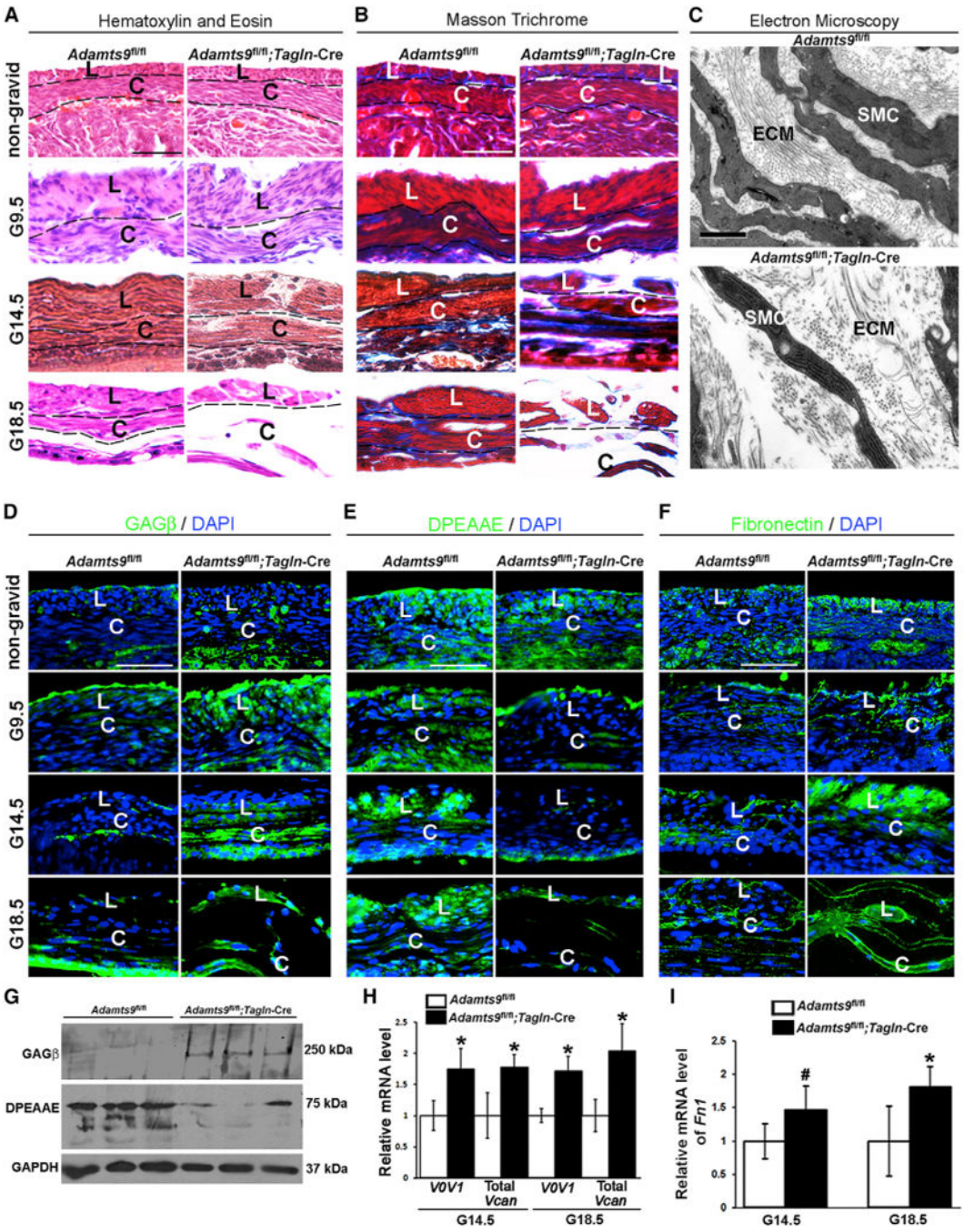

Figure 1. Altered Myometrial Structure and Versican and Fibronectin Dynamics in *Adamts9*-Deficient Myometrium

(A) H&E stain shows myometrial disruption, with increased intercellular space between uterine SMCs in gestational age (G) 14.5 days and G18.5 *Adamts9*$^{fl/fl}$*;Tagln*-Cre uterus.

(B) Masson trichrome stain shows reduced collagen staining (blue) in G18.5 *Adamts9*$^{fl/fl}$*;Tagln*-Cre myometrium.

(C) TEM at G18.5 shows increased intercellular distance between SMCs, sparse collagen fiber bundles, and abundant amorphous non-collagenous matrix in *Adamts9*$^{fl/fl}$*;Tagln*-Cre myometrium.

(D and E) Immunofluorescence showing versican accumulation (anti-GAGβ, green; nuclei stained blue by DAPI) from G9.5 to G18.5 (D) and reduced ADAMTS-cleaved versican (anti-DPEAAE, green) (E) in 3-week-old and gravid *Adamts9*$^{fl/fl}$*;Tagln*-Cre myometrium.
(F) Increased fibronectin staining (green; nuclei stained blue by DAPI) is seen in non-gravid and gravid *Adamts9*$^{fl/fl}$*;Tagln*-Cre myometrium compared with control.
(G) Representative western blots show increased versican (anti-GAGβ) and reduced cleaved versican (anti-DPEAAE) in three *Adamts9*$^{fl/fl}$*;Tagln*-Cre uteri relative to their control littermates.
(H) qRT-PCR shows increased *Vcan* mRNA in *Adamts9*$^{fl/fl}$*;Tagln*-Cre uterus. n = 3. *p ≤ 0.01. V0V1 denotes the two major extra-neural splice variants V0 and V1.
(I) qRT-PCR shows *Fn1* mRNA is increased in the mutant uterus. n = 4. *p ≤ 0.01, $^{\#}$p ≤ 0.05. L, longitudinal myometrial layer; C, circular myometrial layer; ECM, extracellular matrix; SMC, smooth muscle cell.
Scale bars, 50 μm in (A), (B), and (D)–(F) and 1 μm in (C). Error bars indicate SEM. See also Figures S1–S4.

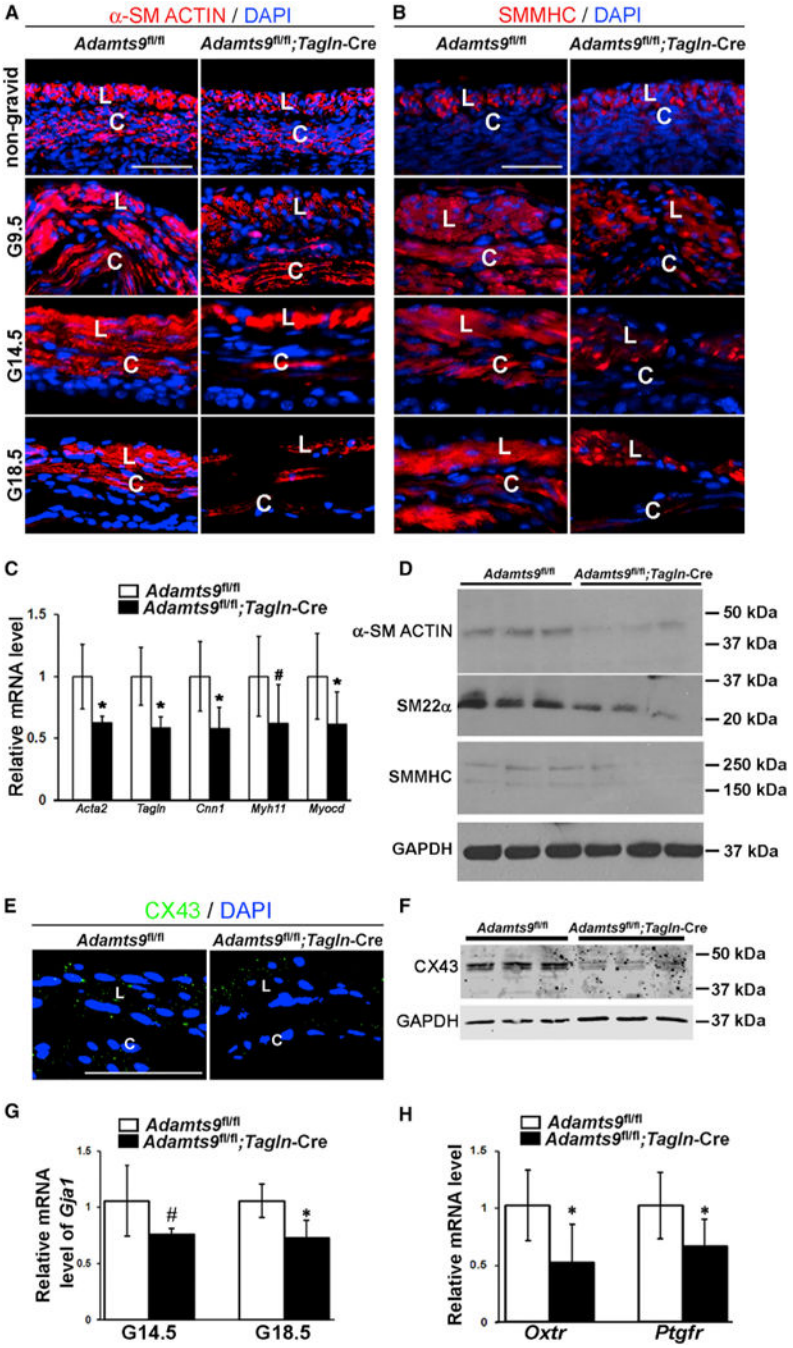

Figure 2. *Adamts9* Deletion Reduces Contractile Protein Content of Myometrial SMCs and Interferes with Gap Junction Formation and Expression of Parturition Hormone Receptors

(A) Reduced staining intensity of smooth muscle a-actin (SMA, red; nuclei, blue) in non-gravid and gravid *Adamts9*$^{fl/fl}$*;Tagln*-Cre myometrium.

(B) Reduced smooth muscle myosin heavy chain staining (SMMHC, red; nuclei, blue) in gravid *Adamts9*$^{fl/fl}$*;Tagln*-Cre myometrium.

(C) qRT-PCR shows reduction of *Acta2*, *Tagln*, *Cnn1*, *Myh11*, and *Myocd* mRNAs in G18.5 *Adamts9*$^{fl/fl}$*;Tagln*-Cre myometrium, compared with control. n = 4. *p ≤ 0.01, $^{\#}$p ≤ 0.05.

(D) Representative western blots for SMA, SM22a, and SMMHC show their reduction in three independent G18.5 gravid *Adamts9*$^{fl/fl}$*;Tagln*-Cre uteri relative to littermate controls. GAPDH was used as a control.

(E) Fewer anti-Cx43 stained speckles (green) indicate fewer gap junctions in *Adamts9*$^{fl/fl}$*;Tagln*-Cre myometrium at G18.5.

(F) Representative western blot shows reduced Cx43 in three pairs of G18.5 *Adamts9*$^{fl/fl}$*;Tagln*-Cre and *Adamts9*$^{fl/fl}$ uterus controls. GAPDH was used as a control.

(G) *Gja1* mRNA levels are reduced in G14.5 and G18.5 *Adamts9*$^{fl/fl}$*;Tagln*-Cre uterus. n = 4. *$p \leq 0.01$, $^{\#}p \leq 0.05$.

(H) Reduced *Oxtr* and *Ptgfr* mRNA in G18.5 *Adamts9*$^{fl/fl}$*;Tagln*-Cre uterus. n = 4. *$p \leq 0.01$. Scale bars, 50 μm. Error bars indicate SEM. See also Figures S2–S4.

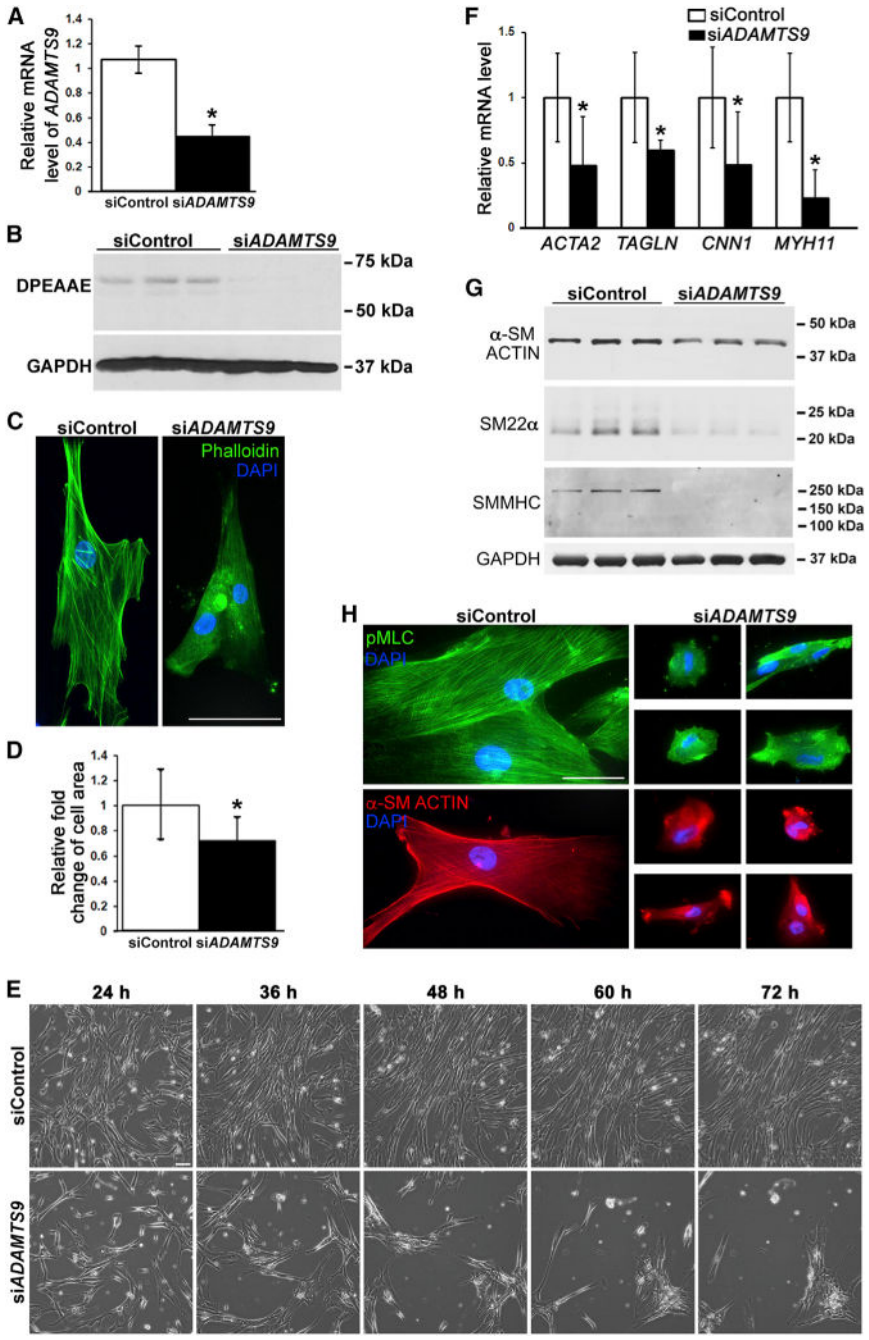

Figure 3. *ADAMTS9* Knockdown Alters HUSMC Shape, Reduces Versican Proteolysis, and Impairs Contractile Protein Expression

(A) qRT-PCR shows reduced *ADAMTS9* mRNA in si*ADAMTS9*-transfected HUSMCs. n = 3. *p ≤ 0.01.

(B) Western blot using anti-DPEAAE antibody shows reduced ADAMTS-cleaved versican in the medium of si*ADAMTS9*-transfected cells. GAPDH was used as a loading control.

(C and D) *ADAMTS9* knockdown reduces stress fiber formation (phalloidin-FITC, green) and impairs cell spreading on plastic (C), quantitatively represented as a reduction of surface area in (D). n = 20. *p ≤ 0.01.

(E) Still images from phase contrast microscopy time-lapse videos (see Videos S1 and S2) of HUSMCs on tissue-culture plastic. In contrast to well-spread control siRNA transfected cells, the si*ADAMTS9*-transfected cells rounded and clumped together 24 hr after transfection until most had detached from the substratum. Contrast with Figure S6B, in which the si*ADAMTS9*-transfected cells are plated on fibronectin.
(F–H) qRT-PCR (F), western blot (G), and immunofluorescence (H) show reduction of smooth muscle contractile gene mRNAs, protein, and staining in HUSMC after *Adamts9* knockdown. n = 3. GAPDH was used as a loading control in (G).*$p \leq 0.01$.
Scale bars, 50 μm. Error bars indicate SEM. See also Figures S5 and S6 and Videos S1 and S2.

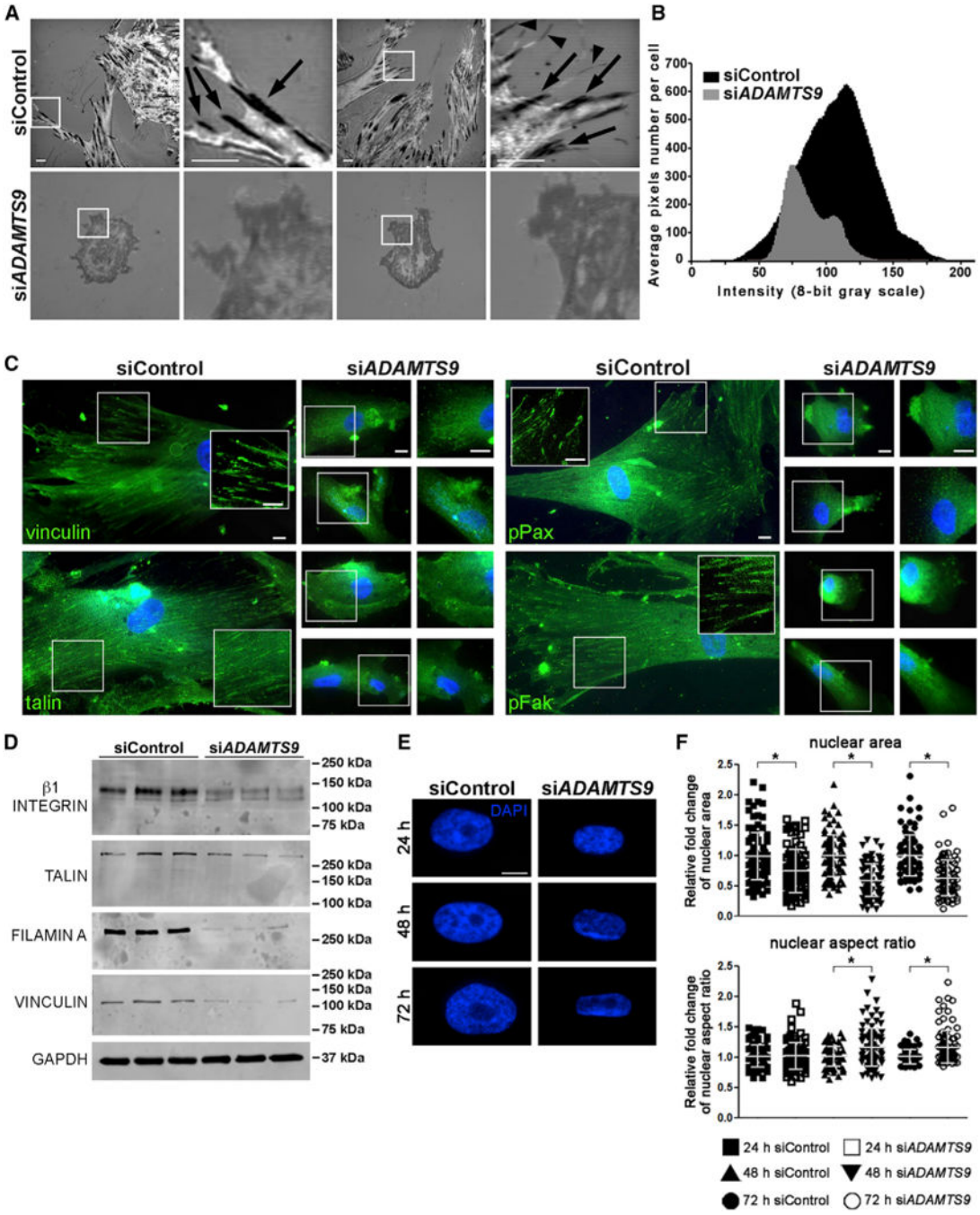

Figure 4. *ADAMTS9* Knockdown Eliminates Focal Adhesions in HUSMC and Alters Nuclear Dimensions

(A) IRM identifies focal adhesions as dark linear regions (arrows) as well as filopodia (arrowheads) at the cell-substratum interface in control siRNA-transfected HUSMC cultures, whereas focal adhesions are poorly formed or absent in si*ADAMTS9*-transfected HUSMC (shown in gray, indicating non-focal close contacts). IRM imaging was done after plating on glass.

(B) IRM image quantification of siControl cells showed a bell-shaped spread of very dark (0) to very light (255) signal, while si*ADAMTS9*-transfected cells have overall dominance

of gray signal intensity with fewer pixels per cell, indicating reduced cell area and an absence of very dark and very bright signal. n = 12 cells.

(C) Reduced staining intensity of focal adhesion components vinculin, talin, phospho (p)-paxillin, and p-FAK (green, nuclei, blue) in si*ADAMTS9*-transfected HUSMCs plated on plastic. The boxed regions with white borders are shown as higher magnification insets or alongside.

(D) Western blots of si*ADAMTS9*-transfected cells show decreased β1 integrin, talin, filamin A, and vinculin, compared with control siRNA-transfected cells. GAPDH is shown as a loading control.

(E and F) DAPI-stained nuclei (E) from control or *ADAMTS9* siRNA-transfected HUSMC plated on plastic were imaged to quantify the nuclear area and aspect ratio, which are significantly different in the two groups (F).

Scale bars, 10 μm. Error bars indicate SEM. See also Videos S3 and S4.

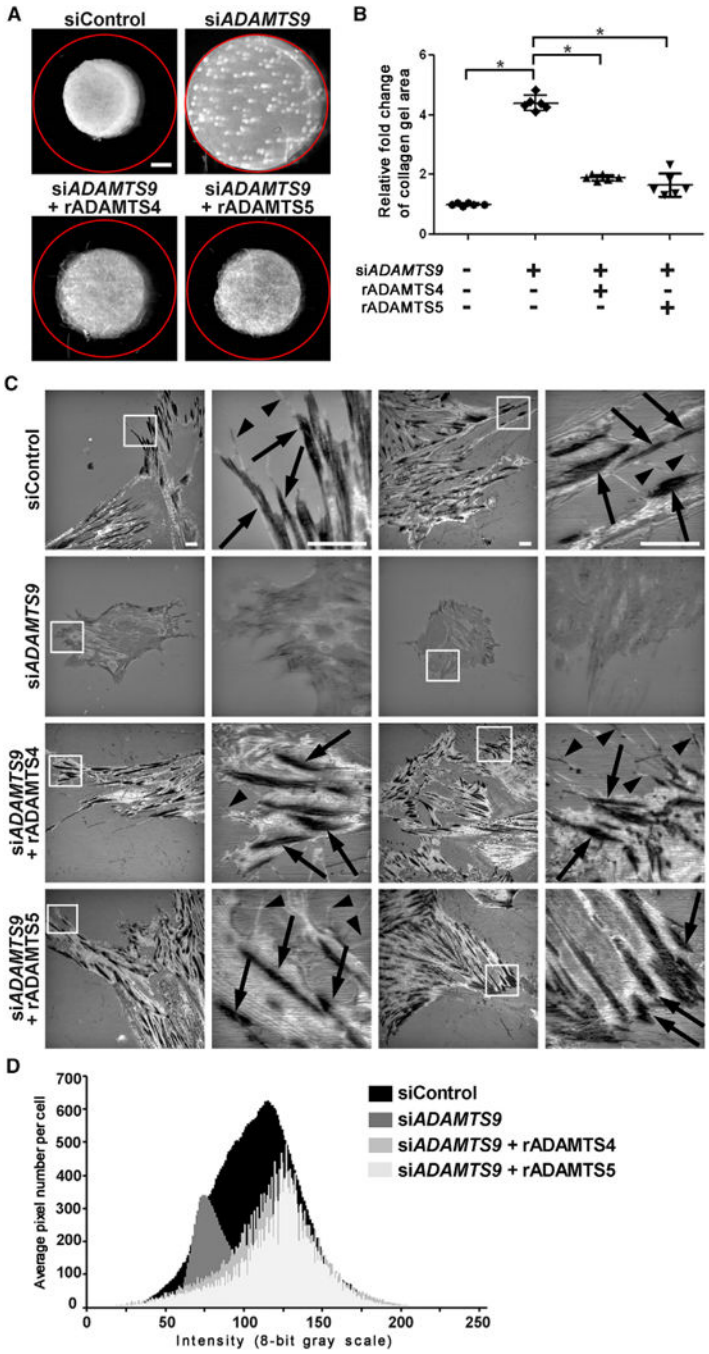

Figure 5. si*ADAMTS9* Impairs Cellular Contractility and Exogenous ADAMTS4 and ADAMTS5 Restore *siADAMTS9*-Induced Changes in Cell Shape, Focal Adhesions, and Contractility

(A) Representative collagen gel contraction assays demonstrate reduced contractility of si*ADAMTS9*-transfected HUSMCs and restoration of contractility after treatment with recombinant ADAMTS4 or ADAMTS5. The red circle indicates the initial size of the collagen gel.

(B) Quantification of gel area demonstrates reduced gel contraction by si*ADAMTS9*-transfected cells and its reversal by addition of exogenous ADAMTS4 or ADAMTS5. Each data point in the plot represents a single gel. n = 6. *p ≤ 0.01.

(C) IRM shows that *ADAMTS9* siRNA severely impairs focal adhesions, seen as dark, linear regions (arrows) in control siRNA-transfected cells and filopodia (arrowheads). These are restored by exogenous ADAMTS4 and ADAMTS5. HUSMCs were plated on glass for IRM.

(D) Quantification of grayscale density in IRM-generated images from n = 10 ADAMTS4 and ADAMTS5-treated cells shows shifts to the left and right that are indicative of normal adhesive interactions and increased pixel numbers indicative of cell spreading. The data for control and si*ADAMTS9*-treated cells are identical to that shown in Figure 4B.

Scale bars, 1 mm in (A) and 10 μm in (C). Error bars indicate SEM. See also Figure S6.

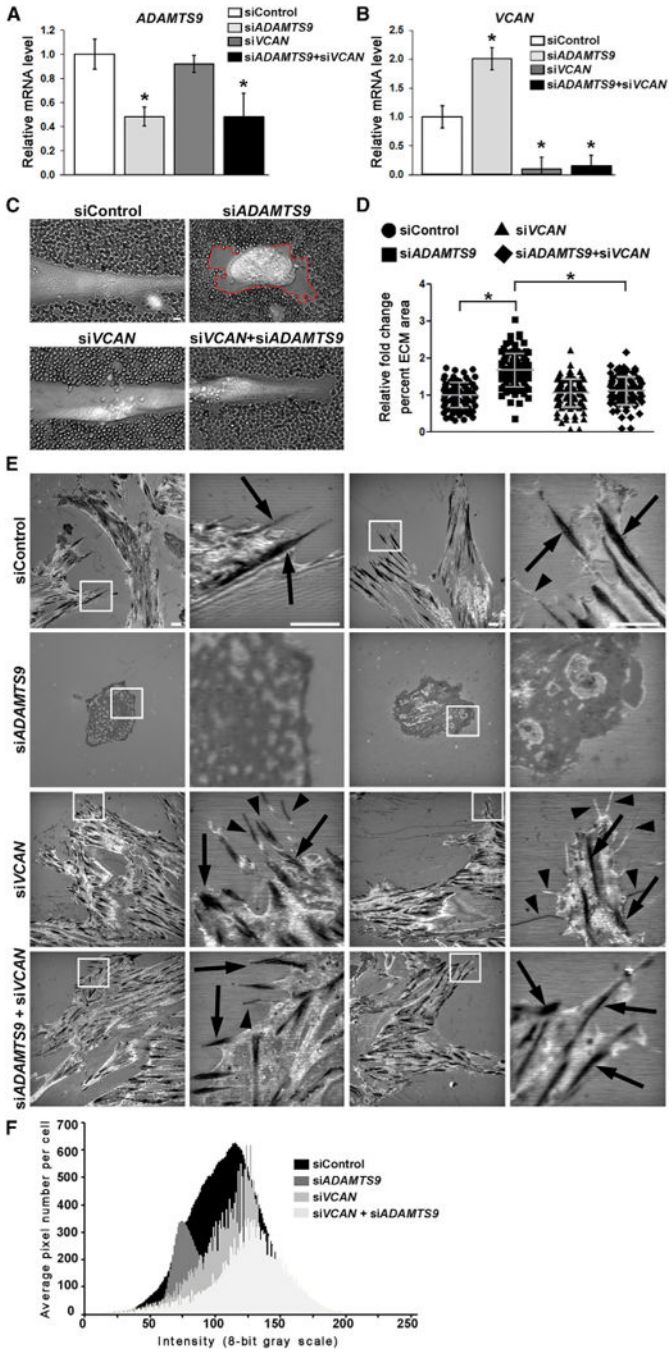

Figure 6. Concurrent Inactivation of VCAN in siADAMTS9-Transfected Cells Restores Normal Pericellular Matrix Dimensions and Formation of Focal Adhesions

For a Figure360 author presentation of Figure 6, see https://doi.org/10.1016/j.celrep.2018.03.034).

(A and B) qRT-PCR illustrates effective knockdown of *ADAMTS9* (A) and *VCAN* (B). Note the statistically significant increase of *VCAN* RNA upon *ADAMTS9* knockdown. *p ≤ 0.01.

(C) Erythrocyte exclusion assay demonstrates increased pericellular matrix around si*ADAMTS9*-transfected HUSMCs (red line). This is restored to normal by si *VCAN*.

(D) Quantification of pericellular matrix area demonstrates a significant increase in si*ADAMTS9*-transfected cells, which is reversed by si *VCAN*. n = 100. *p ≤ 0.01.
(E) IRM shows that co-silencing of *VCAN* and *ADAMTS9* restores focal adhesions (arrows) and filopodia (arrowheads) reduced in si*ADAMTS9*-transfected cells. HUSMCs were plated on glass for IRM.
(F) Quantification of grayscale density in IRM-generated images from n = 10 cells shows shifts to the left and right that are indicative of normal adhesive interactions and increased pixel numbers indicative of increased cell area. The data for control and si*ADAMTS9*-transfected cells are identical to that shown in Figure 4B.
Scale bars, 10 μm. Error bars indicate SEM. See also Figure S6.

Table 1

Observed Incidence of Impaired Parturition

Genotype	***Adamts9*$^{fl/fl}$**	***Adamts9*$^{fl/+}$*; Tagln*-Cre**	***Adamts9*$^{fl/fl}$ *Tagln*-Cre**
Impaired parturition	0	2	14
Number of pregnancies	24	18	18
Frequency	0%	11%	78%